
Mass-Loaded Flows

Julian M. Pittard

School of Physics and Astronomy, The University of Leeds, Leeds, LS2 9JT, UK
jmp@ast.leeds.ac.uk.

1 Introduction

A key process within astronomy is the exchange of mass, momentum, and energy between diffuse plasmas in many types of astronomical sources (including planetary nebulae (PNe), wind-blown bubbles (WBBs), supernova remnants (SNRs), starburst superwinds, and the intracluster medium) and dense, embedded clouds or clumps (e.g., Fig. 1). This transfer affects the large scale flows of the diffuse plasmas as well as the evolution of the clumps. While in much theoretical work this interaction has been ignored, its consequences can be fundamental, as a growing body of literature now shows. Indeed, the standard model of the interstellar medium is based on such exchanges (McKee & Ostriker 1977), which occur through, for example, conduction, ablation and photoevaporation. The injection and mixing of mass from condensations into a surrounding supersonic medium induces shocks, increasing the pressure of the flowing medium (e.g., Pittard et al. 2005). This can lead to clump crushing and the reduction of the Jeans mass causing star formation, and is likely to play a role in sequential star formation (e.g., Elmegreen & Lada 1977), and may allow a starburst to develop (Hartquist, Dyson & Williams 1997). Radiative cooling is one way in which a starburst might be regulated, as it acts to reduce the pressure of the ambient medium once the mass injection rate becomes too high.

Three lengthscales characterize the entrainment of material from a clump into a surrounding flow (Hartquist & Dyson 1993). The smallest lengthscales are associated with the turbulent boundary layer around the clump. On intermediate scales the material injected into the flow forms a cometary-like tail, such as those seen around clumps in PNe. On the largest scales, the material is completely mixed into the flow and becomes indistinguishable from it. Unfortunately, and despite huge effort, the effectiveness of the physical processes in controlling the interchange of dense and diffuse material remains uncertain, in part because of the complexity of the turbulent boundary layers which exist between them. In addition, the microphysics which may drive some global

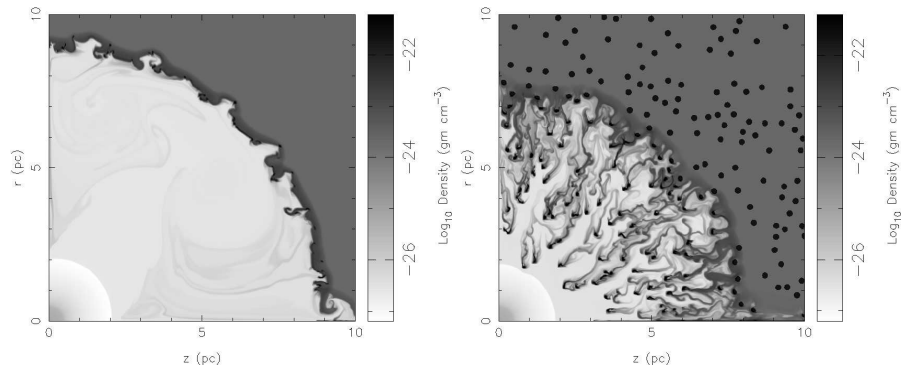


Fig. 1. Numerical simulations which demonstrate the effect of mass-loading on a ‘cluster-wind’ from a group of early-type stars. In the left panel the wind expands into a smooth medium, while in the right panel the ambient medium is clumpy. The time in each simulation is identical. The entrainment of mass from the clumps increases the density of the diffuse gas in the bubble interior, reduces its temperature, and slows its expansion.

processes is poorly understood. For example, magnetic reconnection, which may be necessary in order for clump and diffuse material to fully mix, is a difficult subject.

The influence of John Dyson in the field of mass-loaded flows cannot be overemphasized. He was one of the first to study the process of photoevaporation, he was involved in the development of the widely used analytical theory for ablatively-driven mass-loading, and in many subsequent works he has investigated the effect of mass-loading on a wide variety of astrophysical sources. I am grateful that I have had the opportunity to work with him in this field.

In Sec. 2 I review our current understanding of mass-injection processes. Sec. 3 focuses on intermediate-scale structure, while Sec. 4 examines the global effect of mass-loading on a flow. Sec. 5 concerns the mass-loading of a variety of diffuse sources. For an excellent summary of existing theoretical and observational studies on the interface between clouds and their surroundings see Hartquist & Dyson (1993).

2 Mass Exchange Processes

Consider a cloud of radius r_c , density ρ_c , and mass $M_c = 4/3\pi\rho_cr_c^3$, embedded in a medium of temperature T , density ρ , velocity v , and pressure $P = \rho kT/\mu m_H$. Let c_c and c be the isothermal sound speed in the cold cloud and in the hotter surroundings, respectively, and \mathcal{M} be the Mach number of the flow relative to the cloud. Mass can be lost from the cloud and entrained into the surroundings through three main mechanisms, as discussed in the

following subsections. I describe our current understanding of each process, detail analytical estimates of the rate of mass-loss, and highlight current uncertainties. The mass-loss rates driven by each process are then compared for clumps in a variety of different situations.

2.1 Hydrodynamic Ablation

Numerical simulations of the interaction of a supersonic wind or a strong shock with a single cloud have been presented many times. The evolution for the case of an adiabatic cloud can be broken into 4 consecutive stages: an initial transient stage when the shock first strikes the cloud, a compression stage, a re-expansion stage, and finally a destruction stage. During the initial interaction, a bow shock forms around the cloud, while a shock is driven into the cloud with velocity $v_c \approx \chi^{-1/2}v_s$, where χ is the density ratio between the cloud and its initial (e.g., pre-shock) surroundings, and v_s is the velocity of the shock through the ambient medium. The characteristic timescale for the cloud to be crushed by the transmitted shock is $\tau_{cc} = r_c/v_c \approx \chi^{1/2}r_c/v_s$. When the transmitted shock reaches the back of the cloud, a strong rarefaction is reflected back into the cloud, causing its subsequent re-expansion downstream. This is accompanied by a lateral expansion driven by the high pressure in the cloud and the lower pressure in the surrounding medium at its sides. The cloud is disrupted by the action of both Kelvin-Helmholtz (KH) and Rayleigh-Taylor (RT) instabilities, with the Richtmyer-Meshkov instability playing a minor role unless the surface of the cloud is irregular. Destruction occurs after several crushing times, with the cloud material expanding and diffusing into the ambient flow (Klein, McKee & Colella 1994). In 3-D simulations, instabilities drive a richer structure (Stone & Norman 1992; Xu & Stone 1995). Recent laser experiments confirm that the the vortex ring which forms at the back of the cloud is broken up by the action of azimuthal bending mode instabilities (Klein et al. 2003). In contrast, radiative clouds break up into numerous dense cold fragments which survive for many dynamical timescales (Mellema, Kurk & Röttgering 2002; Fragile et al. 2004). Self-gravity can become dynamically important in the dense fragments behind the compression shock. External magnetic fields generally increase the compression of the cloud and enhance radiative cooling, while magnetic fields internal to the cloud resist compression (see Fragile et al. 2005, and references therein). An example of a numerical calculation of the time evolution of a cold cloud interacting with a supersonic wind is shown in Fig. 2.

An analytical theory for the hydrodynamic ablation of material from dense clumps into the surrounding flow was presented by Hartquist et al. (1986). First, consider a clump embedded in a subsonic flow. The magnitude of the pressure variations over the surface of the clump, created by the well-known Bernoulli effect, is (Landau & Lifshitz 1959)

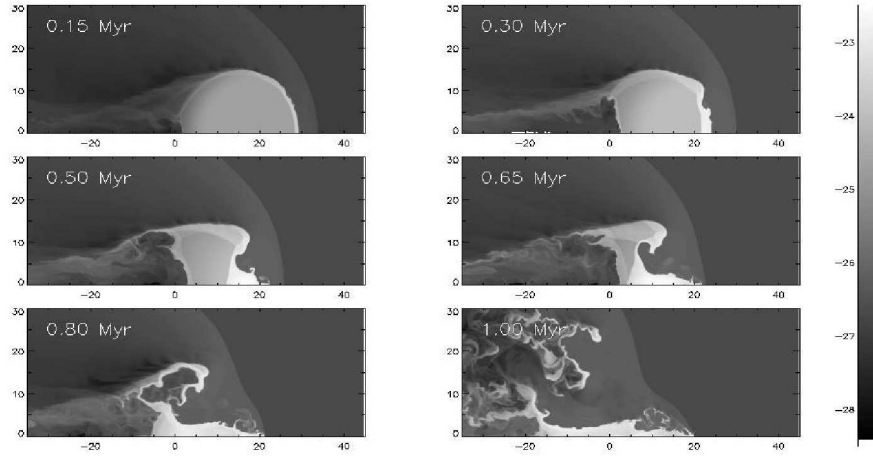


Fig. 2. The destruction of a cold cloud in a supersonic flow by hydrodynamic ablation. The time evolution of the logarithm of mass density is shown (in units of g cm^{-3}), with distances given in pc. At the beginning of the simulation the cloud center is at $z = 20$ pc. $\chi = 500$ and $\mathcal{M} = 3$. There is no thermal conduction or photoevaporation, magnetic fields, or self-gravity, and the simulations are performed using 2D axisymmetry. Radiative cooling is included. (From Marcolini et al. 2005).

$$|\Delta P| \approx P_s \left[1 - \left\{ 1 + \frac{\gamma - 1}{2} \mathcal{M}^2 \right\}^{-\gamma/(\gamma-1)} \right], \quad (1)$$

where the stagnation pressure, $P_s = P + \rho v^2$. In the small Mach number regime, $|\Delta P| \approx \mathcal{M}^2 P_s$. As the flow is fastest at the sides of the clump, the pressure is reduced, and the clump expands in directions normal to the flow at a speed

$$v_{\text{exp}} \approx \frac{\gamma c_c}{\gamma - 1} \ln \left\{ 1 + \frac{\gamma - 1}{2} \mathcal{M}^2 \right\}. \quad (2)$$

For small Mach numbers, $v_{\text{exp}} \approx (\gamma/2)c_c \mathcal{M}^2 \approx c_c \mathcal{M}^2$. Mixing between the cloud material and the flow occurs within a region of size l which is set by the requirement that the rate of mass-loss from the clump, \dot{M}_{ab} , is comparable to the mass-flux of the ambient flow through this region, \dot{M}_s . Since $\dot{M}_{\text{ab}} \sim M_c/t \sim M_c v_{\text{exp}}/l$, and $\dot{M}_s = \rho v l^2$, $l \approx (\mathcal{M}^2 M_c c_c / \rho v)^{1/3}$. In contrast, if the flow is supersonic, mixing occurs largely as a result of a low pressure region over the reverse face of the clump, ‘shadowed’ from the flow. Since the mass cannot leave the clump faster than its sound speed, $v_{\text{exp}} \sim c_c$, and in this case $l \approx (M_c c_c / \rho v)^{1/3}$.

The rate of mass-loss from the clump, $\dot{M}_{\text{ab}} \approx l^2 \rho_l v_{\text{exp}}$, where ρ_l is the characteristic density of ablated material at distance l . Momentum conservation requires that $\rho_l v_{\text{exp}} = \rho v$, so in subsonic flows $\dot{M}_{\text{ab}} \approx \mathcal{M}^{4/3} (M_c c_c)^{2/3} (\rho v)^{1/3}$, while in supersonic flow $\dot{M}_{\text{ab}} \approx (M_c c_c)^{2/3} (\rho v)^{1/3}$ (i.e. independent of \mathcal{M}).

These estimates have received some limited support from the numerical simulations calculated by Klein et al. (1994), although the predicted scaling with the flow parameters remains to be confirmed.

An alternative approach based on ‘mixing-length’ theory has been presented by Cantó & Raga (1991) (see also Arthur & Lizano 1997). While the boundary layer around the cloud is likely to be turbulent, even if the cloud and the surroundings are magnetized (Hartquist & Dyson 1988), such theories are complicated by the unknown degree to which clump gas and the tenuous plasma physically mix, and I do not discuss them further here.

Finally, it is unclear whether the ablation process by itself can merge the stripped material with the global flow in the sense that its temperature, velocity, and density approach those of the surrounding tenuous material. It may therefore be necessary to invoke another process, such as the transfer of heat by thermal conductivity, for the stripped material to acquire the physical state of the surrounding medium. Thermal conduction can accomplish this phase transition without microscopic mixing, and acceleration to the global flow speed is effected by the response of stripped material to pressure gradients and viscous coupling, which may arise from a host of mechanisms including turbulence.

2.2 Conductively-Driven Thermal Evaporation

Cold clouds embedded in a hot medium may also lose mass to their surroundings as hot electrons deposit energy in the surface regions of the clump. This process is referred to as thermal evaporation. The rate of mass loss is dependent on many factors, including the temperature of the hot phase, the clump radius, whether the conductivity is saturated, the presence of magnetic fields and plasma instabilities, and whether there is a velocity difference between the ambient medium and the cloud (e.g., Cowie & McKee 1977; McKee & Cowie 1977). Nonspherical clumps may be treated in an approximate way by adopting half the largest dimension as the radius of the clump (Cowie & Songalia 1977).

If the mean-free-path for electron-electron collisions, λ_{ee} , is approximately less than the temperature scale-height, $T/|\nabla T|$, then the heat flux into the cloud, q , is given by the classical theory of thermal conduction i.e. $q = q_{cl} = -\kappa \nabla T$. The mean-free-path $\lambda_{ee} = t_{ee}(3kT/m_e)^{1/2}$, where the electron-electron equipartition time is given by (Spitzer 1962)

$$t_{ee} = \frac{3m_e^{1/2}(kT)^{3/2}}{4\pi^{1/2}n_e e^4 \ln \Lambda}, \quad (3)$$

where $\ln \Lambda = 29.7 + \ln (T/10^6 \sqrt{n_e})$ is the Coulomb logarithm and the other symbols have their usual meaning. I have implicitly assumed that $T_e = T$. The thermal conductivity, κ , in a fully ionized hydrogen plasma is (see, e.g., Spitzer 1962; Cowie & McKee 1977)

$$\kappa = 1.84 \times 10^{-5} \frac{T^{5/2}}{\ln \Lambda} \text{ erg s}^{-1} \text{ K}^{-1} \text{ cm}^{-1}, \quad (4)$$

(the zero current requirement reduces the effective coefficient of conductivity by a factor ≈ 0.4 - see Spitzer & Härm 1953). The evaporative mass-loss rate from a single clump (Cowie & McKee 1977) is then

$$\dot{M}_{\text{con}} = \frac{16\pi\mu\kappa\omega r_c}{25k} = 2.75 \times 10^{19} \omega r_{\text{pc}} T_6^{5/2} \text{ g s}^{-1} \quad (5)$$

where r_{pc} is the clump radius in parsecs, and $T_6 = T/10^6$ K. For classical evaporation, $\omega = 1$. As conductively driven evaporation has a very temperature sensitive rate, ablation is likely to regulate clump dispersal in lower temperature media.

When $\lambda_{\text{ee}} \gtrsim T/|\nabla T|$, the classical theory of thermal conduction, which is based on a diffusion approximation, may no longer be used. Instead the heat flux reaches a limiting value; i.e. it becomes saturated. The approach to saturated conduction is still partly empirical, and it is common practice to take a flux-limited form for the heat flux: $q_{\text{sat}} = 5\phi\rho c^3$ (Cowie & McKee 1977), where ρ and c are in the hot phase, and ϕ is a parameter of order unity which describes the uncertainty in the numerical value of the saturated heat flux. Observations of the highly saturated solar wind, laboratory plasma experiments, and Fokker-Planck calculations suggest that $0.3 \lesssim \phi \lesssim 1.1$ (Giuliani 1984). Balbus & McKee (1982) conjectured that the effective heat flux, q , can be approximated by the harmonic mean of q_{sat} and q_{cl} ,

$$\frac{1}{q} \approx \frac{1}{q_{\text{sat}}} + \frac{1}{q_{\text{cl}}}. \quad (6)$$

The resulting heat flux reduces to the smaller of the two conduction forms when there is a large disparity between them, and has the convenient property of a smooth transition from diffusive to flux-limited transport. The ratio of classical to saturated heat flux is

$$\sigma = \frac{q_{\text{cl}}}{q_{\text{sat}}} = \frac{\kappa}{5\phi\rho c^3} \frac{dT}{dr}, \quad (7)$$

where the last expression explicitly assumes spherical symmetry i.e. $\nabla T = dT/dr$. The heat flux is then

$$q = \frac{\kappa}{1 + \sigma} \frac{dT}{dr}, \quad (8)$$

where σ is the *local* saturation parameter. This expression becomes the diffusive flux when $\sigma \ll 1$, and the saturated flux when $\sigma \gg 1$.

Cowie & McKee (1977) also defined a *global* saturation parameter,

$$\sigma_0 \equiv \frac{2\kappa T}{25\phi\rho c^3 r_c} = \left(\frac{T}{1.54 \times 10^7} \right)^2 \frac{1}{nr_{\text{pc}}\phi}, \quad (9)$$

where $\ln \Lambda = 30$ has been assumed. Whereas σ measures the saturation locally, σ_0 measures global scales and allows a quick assessment of the importance of saturation effects (σ_0 is essentially the local saturation parameter, σ , evaluated at the ambient conditions with $dT/dr = T/r_c$). For $\sigma_0 \lesssim 0.03/\phi$, radiative losses quench the evaporation, and the clump grows in mass as surrounding material condenses onto it (McKee & Cowie 1977). This, of course, may make the clump gravitationally unstable, and initiate new star formation. For $0.03/\phi \lesssim \sigma_0 \lesssim 1$, the clump is evaporated at the classical rate. The onset of saturation occurs when σ_0 is of order unity, with highly saturated flows having $\sigma_0 \gg 1$. The mass-loss rate in the saturated regime is specified with $\omega \approx (1 + \sigma_0)^{-0.7}$ (Giuliani 1984). Since the onset of saturation is dependent on the radius of the clump for a specified hot phase, larger clumps will tend to evaporate in the classical limit, while the evaporation of mass from smaller clumps will tend towards saturation. If the temperature and density of the hot phase is evolving (e.g., because it is the interior of a WBB or SNR), the radius of clumps which are just at the onset of saturation will also change.

The dynamics of the evaporation process have been analyzed by McKee & Cowie (1975) and Cowie & McKee (1977), and an analogy with ionization fronts can be made. For classical evaporation (i.e. $0.03 \lesssim \sigma_0/\phi \lesssim 1$), the velocity of the conduction front, $v_{\text{cond}} \sim 2\sigma_0\phi c_c^2/c$. If $\sigma_0 \gtrsim 0.25/\phi$, the conduction front drives a shock into the cloud. Otherwise, the cloud evaporates subsonically. Conduction fronts in the saturated regime have a velocity $v_{\text{cond}} \sim 1.12\sigma_0^{1/8} c_c^2/c_w$ (for $\phi = 1$), and always drive a shock into the cold cloud ahead of the conduction front itself.

Time-dependent hydrodynamical simulations of clouds overrun by a strong shock and undergoing conductively-driven thermal evaporation in the classical regime have been calculated by Orlando et al. (2005). Conduction inhibits the growth of Rayleigh-Taylor and Kelvin-Helmholtz instabilities, and the fragmentation of the cloud, but heats the evaporated material so that it quickly becomes part of the ambient flow. Simulations in the saturated regime confirm that the conduction front initially drives a shock into the cloud (Ferrara & Shchekinov 1993; Marcolini et al. 2005), substantially increasing its density. The resulting evolution then appears sensitive to assumptions concerning the cooling, with the cloud and the evaporation either settling into a quasi-steady-state (Ferrara & Shchekinov 1993), or displaying oscillatory behaviour (Marcolini et al. 2005). The mass-loss rate during the initial phase is comparable to that inferred from Eq. 5, but it is substantially reduced as the cloud is compressed and decreases in size (Marcolini et al. 2005). Somewhat different models including self-gravity have been calculated by Vieser & Hensler (2000) and Hensler & Vieser (2002).

Conductively-driven evaporation is perhaps the best-studied of the three processes highlighted in this section, but there are uncertainties in many physical processes whose influence on \dot{M}_{con} remains poorly quantified. For instance, when $\sigma_0 \gtrsim 100$, viscous stresses have the potential to increase \dot{M}_{con} significantly, but the exact enhancement depends on the uncertain degree

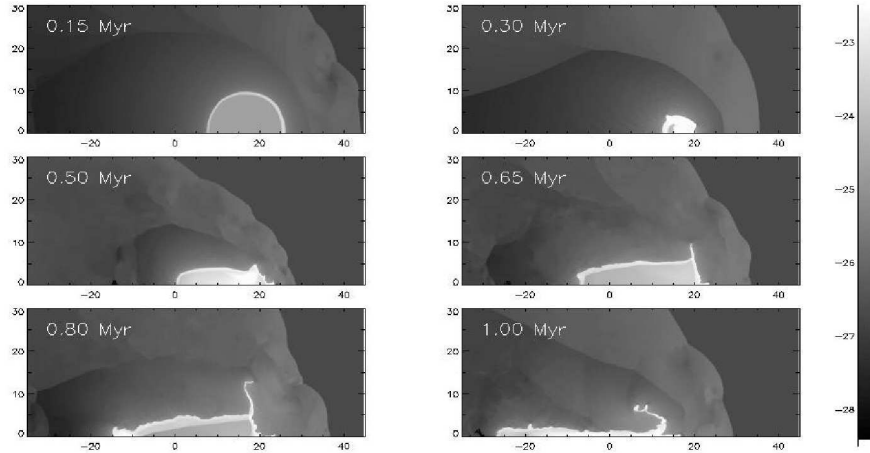


Fig. 3. As Fig. 2, but with heat conduction in the saturated regime ($\sigma_0 = 16$). A strong shock is driven into the cloud ahead of the conduction front and compresses it from all sides, so that its radius has decreased by a factor of 3 by $t = 0.3$ Myr. The subsequent evolution is also markedly different from the purely hydrodynamical case. (From Marcolini et al. 2005).

to which they might also saturate (Draine & Giuliani 1984). On the other hand, if the electron mean free path is reduced, the heat flux will be inhibited. Bandiera & Chen (1994a,b) have emphasized that when $\sigma_0 \gtrsim 100$, the requirement of a zero net current means that hot electrons are stopped by electrostatic effects within a thin surface layer. The resulting heat flux is then considerably lower than that obtained if the electrons penetrate deep into the cloud and directly heat it through Coulomb collisions (Balbus & McKee 1982). The electron mean free path can also be reduced as a result of scattering by plasma instabilities, such as the ion-acoustic instability (Galeev & Natanzon 1984), and by whistler waves (Gary & Feldman 1977; Levinson & Eichler 1992). However, it is difficult to obtain a self-consistent model of these processes, and the presence of a strong magnetic field may suppress such instabilities. Partial ionization and non-equilibrium cooling are other possibilities for suppressing the conductivity (Böhringer & Hartquist 1987). Magnetic fields may not reduce the conductivity as much as previously thought (e.g., Balbus 1986; Rosner & Tucker 1989; Cho et al. 2003) unless the cloud is magnetically disconnected from its surroundings. An example of a numerical calculation of the time evolution of a conductively-evaporating cold cloud interacting with a hot supersonic wind is shown in Fig. 3.

2.3 Photoevaporation

The fate of a neutral clump exposed to a strong ionizing radiation field has been extensively studied over the years. Small, low-mass clumps are instantly ionized and rapidly dissipate i.e. are ‘zapped’. In contrast, clouds which are sufficiently dense and large trap the ionization front, which becomes D-critical (Dyson 1968; Bertoldi 1989) and moves into the cloud driving a shock front ahead of it. The ionized gas streams away perpendicular to the ionization front and expands supersonically into the interclump medium, reaching an asymptotic Mach number of ≈ 2 (e.g., Kahn 1969). This flow may absorb a large part of the incident ionizing flux and appear as a bright rim to the clump. The shock driven into the clump is focussed onto the clump axis, and can substantially increase the initial clump density (Sandford, Whitaker & Klein 1982). This ‘radiation-driven implosion’ may make the clump gravitationally unstable and lead to new star formation. Otherwise, the pressure overshoot causes the clump to reexpand, and it undergoes several radial oscillations (Lefloch & Lazareff 1994) before obtaining an equilibrium, cometary-shaped structure (Bertoldi & McKee 1990). Recombination may occur in the shadow of the clump, but this is prevented if there is a diffuse component to the radiation field (Pavlakis et al. 2001). The pressure in the evaporating flow declines rapidly, and eventually a termination shock forms. If the surrounding medium is supersonic a bow-shock is also formed. Photoevaporated flows also occur from the neutral disks which surround pre-main-sequence stars, known as ‘proplyds’ (O’Dell, Wen & Hu 1993; Bally et al. 1998).

Analytical equations for the mass injection rate of the photoevaporated flow as the clump is destroyed are presented in Bertoldi (1989) and Mellema et al. (1998). Good agreement with results from numerical simulations is obtained. However, it is possible to obtain a simple estimate by setting $\dot{M}_{\text{ph}} = mFA$, where m is the mass per particle of the neutral material, and F and A are respectively the rate per unit time per unit area at which hydrogen ionizing photons reach the ionization front and its area. F is reduced by absorptions in the photoevaporating flow, and is approximately given by (Mellema et al. 1998)

$$F \approx \frac{F_0}{(1 + \alpha_B F_0 r_{\text{if}} / 3c_i^2)^{1/2}}, \quad (10)$$

where $\alpha_B = 2.6 \times 10^{-13} \text{ cm}^3 \text{ s}^{-1}$ is the case B recombination rate for H, r_{if} is the radius of curvature of the ionization front, c_i is the isothermal sound speed of the ionized gas, and $F_0 = \dot{S}/4\pi d^2$ is the flux delivered by the ionizing sources at the position of the clump. Typical assumptions are $r_{\text{if}} \approx r$ and $A \approx \pi r^2$. \dot{M}_{ph} declines with time as the clump is destroyed and r decreases.

Photoevaporation may be suppressed if the ram or thermal pressure of the surrounding medium is greater than the pressure of the evaporating flow (Dyson 1994). Density inhomogeneities within the clump may affect the process of photoevaporation, as may the instability of inclined ionization fronts

(Williams 2002). The role of magnetic fields on the structure of ionization fronts (Williams et al. 2000) may also affect \dot{M}_{ph} .

2.4 Comparison of Mass-Injection Rates

While the exact rates of mass-loss by the three processes described in Sec. 2.1-2.3 remain somewhat uncertain, an appreciation of their relative importance can be obtained by considering several different objects.

The Helix Nebula (NGC 7293)

The Helix Nebula is famous for containing many extended cometary tail-like structures, which emanate from dense, neutral globules, and point away from the central star. The clumps have on average the following properties: $r_c \approx 10^{-3}$ pc, $T_c \approx 10$ K, $n_c \approx 10^6$ cm $^{-3}$ (Dyson et al. 1989). A typical distance of a clump from the central ionizing star is $d \approx 0.1$ pc. The star has an ionizing photon flux $\dot{S}_{49} = \dot{S}/10^{49} \approx 3.5 \times 10^{-4}$. The clumps appear to be overrun by [OIII] gas with $T \approx 10^4$ K, $n \approx 10^3$ cm $^{-3}$, and a relative velocity, $v \approx 17$ km s $^{-1}$ (Meaburn et al. 2005). Hence, the Mach number of the flow relative to the clumps is about 1.5. Using the analytical equations in Secs. 2.1 through to 2.3, we determine that $\dot{M}_{\text{ab}} \approx 1.6 \times 10^{16}$ g s $^{-1}$ and $\dot{M}_{\text{ph}} \approx 2.4 \times 10^{17}$ g s $^{-1}$. The global saturation parameter, $\sigma_0 \approx 4 \times 10^{-7}$ for $\phi = 1$, and gas would like to condense onto the clumps at a rate $\dot{M} \approx 2 \times 10^{16}$ g s $^{-1}$ (Cowie & McKee 1977), though this is likely prevented by the mass-loss that occurs through photoevaporation and ablation. The estimated lifetime of such clumps is in excess of 4×10^4 yr, compatible with the estimated age of the nebula. The origin of the knots is discussed in Dyson et al. (1989).

The Wolf-Rayet Nebula RCW 58

RCW 58 is a nebula surrounding the Wolf-Rayet star WR 40, and which has been formed by the current stellar wind sweeping up wind material from previous evolutionary stages, some of which is clumpy (Chu 1982; Smith et al. 1988). The clumps are ionized by the central star and typically have the following properties: $r_c \approx 0.1$ pc, $T_c \approx 10^4$ K, $n_c \approx 10^3$ cm $^{-3}$ (Arthur, Henney & Dyson 1996). They are embedded in shocked stellar wind material, with $n \approx 1$ cm $^{-3}$, $v \approx 200$ km s $^{-1}$. The flow around the clumps has $\mathcal{M} \approx 0.6$. The H-ionizing flux from the star is $\dot{S}_{49} \approx 2.5$ (P. Crowther, private communication). For clumps at a distance of 1 pc from the star, $\sigma_0 \approx 4$, and the conductivity-driven mass-loss is mildly saturated with $\dot{M}_{\text{con}} \approx 3 \times 10^{20}$ g s $^{-1}$. A higher mass-loss rate is obtained for ablation: $\dot{M}_{\text{ab}} \approx 10^{21}$ g s $^{-1}$. Since the cloud is already ionized it does not make sense to calculate a photoevaporation rate, but this may once have been the dominant process if the cloud was formerly neutral. Therefore, ablation would appear to control the rate at which mass is currently stripped from the clump.

Within a WBB

Of course, the mass-loss rate from each process varies within a bubble as the density, velocity, temperature, and distance from the ionizing source change. This is demonstrated in Fig. 4, where the top panel shows an example of the density and temperature structure within a bubble, while the mass-loss rates and lifetime of a specific clump are shown in the bottom panel.

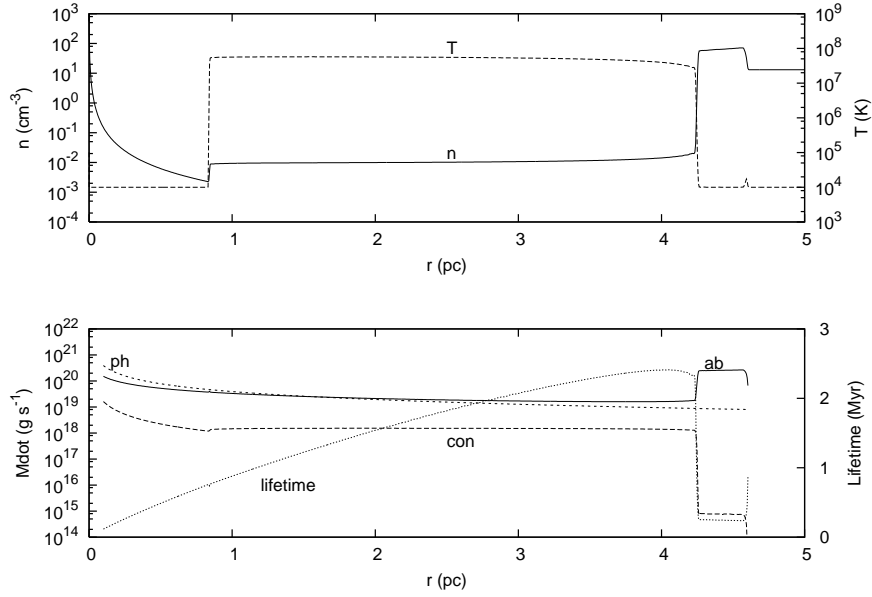


Fig. 4. Top: The internal structure (total number density and temperature) of a WBB of age 0.1 Myr expanding into a stationary medium with $n_{\text{H}} = 10 \text{ cm}^{-3}$. The central star has $\dot{M} = 10^{-6} M_{\odot} \text{ yr}^{-1}$, $v_{\infty} = 2000 \text{ km s}^{-1}$, and $\dot{S}_{49} = 1.2$. Bottom: The mass-loss rate from clumps of radius 0.01 pc, $n = 10^7 \text{ cm}^{-3}$, $T = 100 \text{ K}$, due to hydrodynamic ablation (ab), photoevaporation (ph), and conductively-driven evaporation (con). No clumps are assumed to reside within the central 0.1 pc of the bubble. Clumps located within the hypersonic stellar wind are assumed to be surrounded by a sheath of hot gas bounded by a bowshock on their windward surface. The conductively-driven evaporation is highly saturated for clumps within the hot gas of the bubble given the parameters chosen, but is in the condensational regime within the shell of swept-up ambient material. Also shown is an estimate for the lifetime of the clumps: $t = (\dot{M}_{\text{ab}} + \dot{M}_{\text{con}} + \dot{M}_{\text{ph}})/M_{\text{c}}$.

3 Intermediate-Scale Structure

While the stripping of mass from clumps has been extensively, though not definitively studied, to date there has been very little work on how intermediate-scale structures disperse/merge into the background flow. This problem has received some attention in studies of the interaction between multiple clouds and a flow (e.g., Jun, Jones & Norman 1996; Poludnenko, Frank & Blackman 2002; Steffen & López 2004), but our understanding of such interactions is still developing. A limitation of these works is that the clumps have been modelled as single-phase entities, and the density contrast between the clumps and their surroundings has, for numerical reasons, typically been $\sim 10^2$. The simulated clumps then have such short lifetimes that they are unable to significantly mass-load the flow. In reality, in many astrophysical flows the density contrasts are much larger. A different numerical approach which accounts for the much longer lifetimes of clumps is to set up sources which continuously inject mass into the flow (Falle et al. 2002). Multiple sources act as an efficient barrier to the flow if they are sufficiently close together that their combined mass injection rate is comparable to or exceeds the mass flux of the incident flow into the volume that they occupy (Pittard et al. 2005, see also Fig. 5). In such cases, the thermal pressure of the flow is greatly enhanced (at the expense of its ram pressure), and crucially becomes relatively uniform - these conditions are exactly those required to increase the probability of cloud collapse and new star formation.

Perhaps one of the best examples of intermediate scale structure is the comet-like tail extending from the Galactic Centre source IRS 7, a red supergiant (Yusef-Zadeh & Morris 1991; Serabyn, Lacy & Achtermann 1991). Although originally interpreted in terms of a global wind-wind collision between the slow dense wind from IRS 7 and a Galactic wind, this model had difficulty in explaining the length of the tail (Yusef-Zadeh & Melia 1992). However, it may be overcome if the wind of IRS 7 is clumpy enough that it becomes semiporous to the Galactic wind, with much smaller bow-shocks forming around each clump (Dyson & Hartquist 1994).

4 The Global Effect of Mass-Loading on a Flow

The effect of mass-loading on a global flow can be studied in a one-fluid approximation if the following two assumptions are made: i) the clumps are sufficiently numerous that they can be considered to be continuously distributed; ii) the characteristic scale length of injection and mixing is much smaller than the dimensions of the global flow (so that the injected mass reaches the general flow velocity and temperature essentially instantaneously). For the steady injection of mass from an ensemble of clumps into the interior of a spherically expanding flow, the time-independent continuity and momentum equations are then

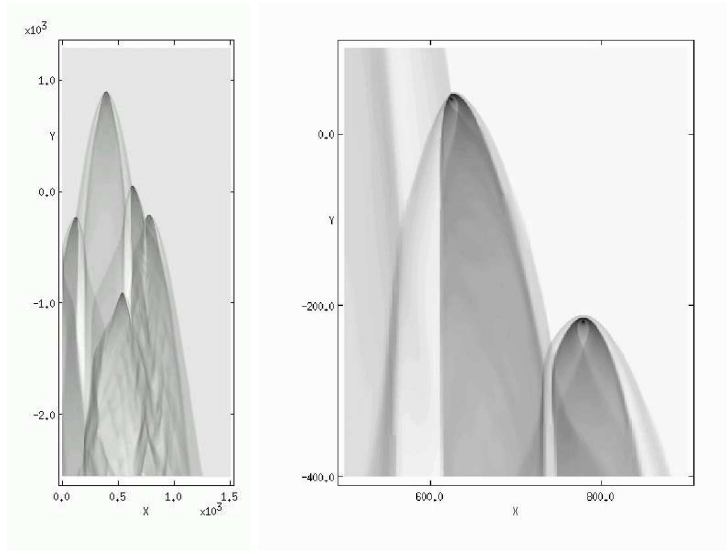


Fig. 5. The interaction of a hypersonic flow with multiple cylindrical mass sources when the combined mass injection rate is comparable to the mass flux of the incident flow through the volume that the mass sources occupy (from Pittard et al. 2005). The right panel shows an enlargement of the flow around two of the mass sources.

$$\frac{1}{r^2} \frac{\partial(r^2 \rho u^2)}{\partial r} = Q \quad (11)$$

and

$$\rho v \frac{\partial v}{\partial r} + \frac{a^2}{\gamma} \frac{\partial \rho}{\partial r} + \frac{2\rho a}{\gamma} \frac{\partial a}{\partial r} = -Qv, \quad (12)$$

where r is the distance from the star, and a is the isothermal sound speed of the flow. Q is the mass loaded into the flow per unit time per unit volume. The clumps are assumed, on average, to be stationary with respect to the global flow, so that there is no net rate of momentum injection.

The continuity and momentum equation may be combined to give

$$(v^2 - a^2) \frac{\partial v}{\partial r} = -\frac{Q}{\rho} (v^2 + a^2) + \frac{2a^2 v}{r}. \quad (13)$$

If r is large (i.e. the flow is plane-parallel) and if $v > a$ (i.e. $M > 1$), then $v^2 > a^2$, $\partial v / \partial r < 0$, and the flow decelerates. On the other hand, if r is large and $v < a$ (i.e. $M < 1$), then $v^2 < a^2$, $\partial v / \partial r > 0$, and the flow accelerates. A key feature of mass-loading is that it tends to drive the ambient flow to Mach number unity (Hartquist et al. 1986). For an expanding, time-dependent flow, mass-loading may drive the Mach number to 0.6-0.7 (Arthur, Dyson & Hartquist 1993). Another feature is that if mass-loading is large, a global reverse shock will be greatly weakened

(Arthur, Dyson & Hartquist 1994; Williams, Hartquist & Dyson 1995; Williams, Dyson & Hartquist 1999; Pittard, Hartquist & Dyson 2001b). In addition, a two-fluid study has revealed that shocks which overrun clumpy media are weakened and broadened (Williams & Dyson 2002). This has significant implications for the survival of the clumps. Finally, the injection of mass into a radiative medium has a stabilizing influence against isobaric and isentropic perturbations, and can suppress the development of the thermal instability (Pittard et al. 2003).

5 Sources with Large-Scale Mass-Loaded Flows

Theoretical studies of the effect of mass-loading on a flow fall into two categories. If the flow is treated as a single fluid and has a very simple geometry, it is often possible to obtain a similarity solution. Alternatively, one can use a hydrodynamical code to model and find a wider variety of solutions. This allows much greater flexibility, and the ability to incorporate a larger number of physical processes. In principle, a two-fluid approach can be used, in which a time-dependent spectrum of clumps is separately tracked. Of course, an unavoidable drawback of such computations is the loss of generality, as, for instance, the clump spectrum inside a starburst superwind is likely to be somewhat different to that in our local ISM.

In the following subsections I discuss mass-loading in a variety of astrophysical settings. The properties of winds mass-loaded by material from clumps (or stellar sources) has also received theoretical attention in the context of ultracompact H II regions (Dyson, Williams & Redman 1995), Herbig-Haro objects (see discussion in Hartquist & Dyson 1988, 1993), and globular cluster winds (Durisen & Burns 1981). The mass-loading of accretion flows in stellar clusters and AGNs has also been studied by David & Durisen (1989) and Toniazzo, Hartquist & Durisen (2001).

5.1 WBBs, PNe, and Superbubbles

The dramatic and beautiful impact of stellar winds on their environment has long been recognized (e.g., see the chapter by Jane Arthur). The first similarity solutions of this interaction, which assumed a smooth wind and environment, were obtained by Dyson & de Vries (1972) and Dyson (1973). The shocked ambient gas was found to cool very rapidly (as subsequently shown in a numerical simulation by Falle 1975), and the hot shocked wind was found to fill most of the bubble volume. The effect of mass-loading was first considered by Weaver et al. (1977), who obtained an approximate similarity solution for a WBB expanding into a constant density medium by assuming an isobaric shocked wind region. In this work, mass-loading of the interior of the WBB is assumed to occur through the conductively-driven evaporation of the cool swept-up shell. The mass transferred into the bubble interior may easily dominate the total mass within the bubble. Hanami & Sakashita (1987)

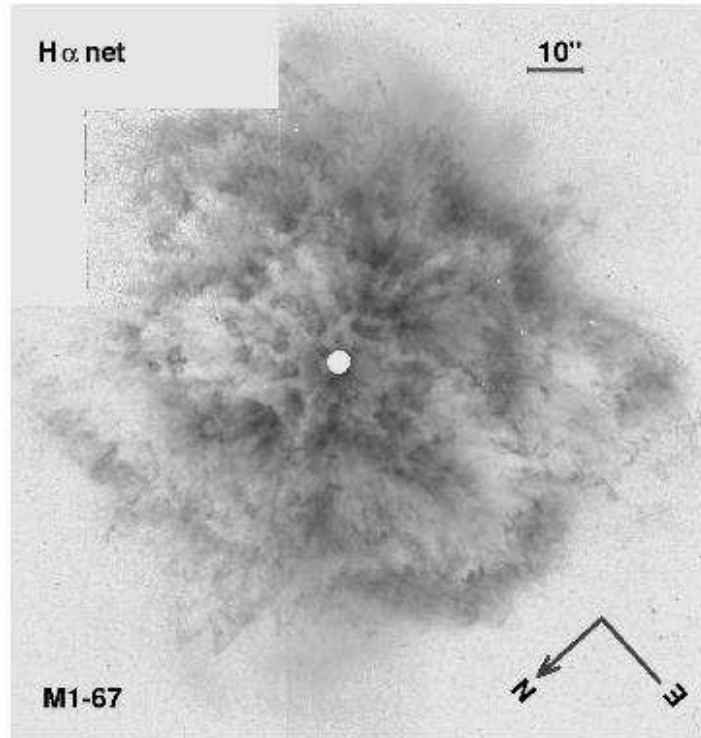


Fig. 6. The M1-67 nebula around WR 124. This is the youngest known WR nebula, and unlike older nebulae there is no obvious global shell surrounding a central cavity. Instead, the interaction between the current wind and its LBV progenitor starts close to the central star and extends to the outer boundary (reproduced from Grosdidier et al. 1998).

used this same approach to generalize the Weaver et al. (1977) model to an ambient density with a power-law slope, as well as considering the conductive evaporation of embedded clumps. An analytical solution based on the Weaver et al. (1977) model for WBBs in a density gradient was obtained by García-Segura & Mac Low (1995). Similarity solutions of WBBs mass-loaded by embedded clumps and obtained without the assumption of a constant pressure shocked wind were described by Pittard, Dyson & Hartquist (2001a) and Pittard et al. (2001b). A similarity solution analogous to the Weaver et al. (1977) model, but taking into account the time-dependence of the stellar wind, was obtained by Zhekov & Perinotto (1996), while Zhekov & Myasnikov (1998) derived a similarity solution (based on the Weaver et al. (1977) model) with reduced thermal conduction.

Some of the best studied WBBs are around WR stars. Many of these display a clumpy morphology, and mass-loading is likely to be an important

process. Evidence for mass-loading in WBBs was obtained by Smith et al. (1984), who observed a correlation between the velocity and ionization potential of ultraviolet absorption features towards the central star of the RCW 58 WBB. The slope of this relationship effectively measures the ratio of the mass flux to the pressure in the line-forming region, i.e. $\rho v/P$, and the value of this ratio implies that the rate of mass loading into the bubble is 40-50 times greater than the mass-loss rate of the WR star (Hartquist et al. 1986). A standard bubble without mass-loading is unable to explain the wide range of observed velocities, while the Weaver et al. (1977) model predicts a correlation of the opposite sense, irrespective of the assumed ambient density gradient (see Hanami & Sakashita 1987). In contrast, similarity solutions with mass loading from embedded clumps *are* able to reproduce this correlation (Hanami & Sakashita 1987; Pittard et al. 2001a,b), as can hydrodynamical simulations of the same process (Arthur et al. 1993, 1996). Further evidence for mass-loading in wind-blown bubbles is provided by spectroscopic data of core-halo PNe, which indicate halo temperatures in excess of that which can be obtained by photoionization alone (Meaburn et al. 1991). Dyson (1992) and Arthur et al. (1994) have shown that this is consistent with a transonic wind leaving a mass-loaded core region and shocking against clumps in the halo region.

Without some form of mass-loading, the hot gas in WBBs, PNe, and superbubbles may be too rarefied to produce observable X-ray emission. Irrespective of the entrainment process, mass-loading increases the interior density of the bubble while simultaneously reducing its temperature (the same thermal energy must now be shared between more particles), and as a consequence, the X-ray emission both softens and dramatically increases. We are therefore fortunate that the last three decades have been a golden age of X-ray astronomy, with the operation of successive facilities with vastly improved sensitivity, spatial- and energy-resolution. The observed temperatures in WBBs, PNe, and quiescent (i.e. those without recent SNe) superbubbles are all reasonably soft and therefore indicative of mass-loading (though other explanations are also possible). However, applications of the Weaver et al. (1977) and García-Segura & Mac Low (1995) models predict far too much X-ray emission (sometimes by a factor of 100), so at the very least the evaporation of mass from a dense swept-up shell must occur at a much reduced rate.

Only two WBBs have been detected to date at X-ray energies, NGC 6888 (Wrigge 1999) and S308 (Chu et al. 2003), both of which are limb-brightened. At first, this morphology seems to agree with the predictions of the Weaver et al. (1977) and García-Segura & Mac Low (1995) models since the emissivity is highest where the density is highest and the temperature lowest. However, the soft emission from the limb is easily absorbed by the ISM, with the result that such models predict a centre-filled appearance (Wrigge et al. 2005). Again, a reduction in the conductivity can improve the level of agreement. It remains to be seen whether bubbles with distributed mass-loading from embedded clumps can better reproduce the observed limb-brightening, though

this process has some support from hydrodynamical simulations which often show instabilities breaking dense clumps off cold swept-up shells and subsequently becoming entrained in the hot bubble interior (e.g., see Fig. 6 in the chapter by Jane Arthur). An alternative explanation is that the X-ray emission from NGC 6888 and S308 arises from the shocked RSG wind, and is currently enhanced in these objects by a collision between the WR and RSG shells (Freyer, Hensler & Yorke 2006). However, this requires that the RSG wind is fast ($\sim 100 \text{ km s}^{-1}$), and speeds of this order are far from certain (see discussion in García-Segura, Langer & Mac Low 1996). Finally, there is a vast amount of evidence that the stellar winds themselves are clumpy, which has further implications for their interaction (see, e.g., Fig. 6).

Discerning the morphology of PNe is more difficult, as their angular size is smaller. Only Mz 3 and NGC 6543 are adequately resolved, and, like the WBBs around massive stars, are limb-brightened (Chu et al. 2001; Kastner et al. 2003). Unlike the WBBs around massive stars, internal absorption within the nebula is likely to be important, while the action of collimated outflows and heat conduction may also modify the observed X-ray morphology (Kastner et al. 2002). The duration for the presence of hot gas appears to be short, as only young PNe show diffuse X-ray emission.

On larger scales, the combined action of stellar winds and SNe from massive stars in OB associations sweep up the ambient ISM to form superbubbles. The physical structure of a superbubble is expected to be similar to that of a WBB formed around an isolated massive star. Superbubbles containing recent SNe have X-ray luminosities which exceed the predictions from the Weaver et al. (1977) model, but when in a quiescent state (i.e. without recent SN blasts) the X-ray luminosities are an order of magnitude lower than expected from the Weaver et al. (1977) model (Chu et al. 1995). In contrast to WBBs and PNe, quiescent superbubbles have a center-filled X-ray morphology, with brighter X-ray emission near the central star cluster, and hotter gas ($T \sim 10^7 \text{ K}$). The diffuse X-ray emission from high-mass star-forming regions has also been studied on smaller scales (see, e.g., Townsley et al. 2003). In M17, it appears that the hot plasma is mass-loaded by a factor of ~ 10 (Dunne et al. 2003). However, other processes, such as particle acceleration, and different electron and ion temperatures may also be important.

An interesting finding for clump-embedded, conductively-driven mass-loading is the occurrence of a negative feed-back mechanism, which sets a maximum limit to the amount that a bubble can be mass-loaded (Pittard et al. 2001a). This arises as a consequence of the dependence of the evaporation rate on temperature and the lowering of temperature by mass loading. Since mass-loading to primary stellar wind mass ratios approaching those inferred for RCW 58 could not be obtained, a key conclusion is that ablation from embedded clumps must be the dominant driver of mass-injection in RCW 58 in particular, and perhaps also more generally (this finding is in agreement with the estimate that $\dot{M}_{\text{ab}} > \dot{M}_{\text{con}}$ in Sec. 2.4). However, the lower mass-loading

to primary stellar wind mass ratios deduced for S308 and M17 probably do not rule out conductively-driven mass-loading in these sources.

5.2 SNRs and Starburst Superwinds

The fact that the ISM is known to be multi-phase means that SNRs are undoubtedly mass-loaded, and there is clear observational evidence of engulfed clumps within the SNR N63A (Chu et al. 1999; Warren, Hughes & Slane 2003). Young SNRs first interact with the circumstellar material ejected by their progenitor. The youngest SNR in the Galaxy, Cas A, contains bright, slow-moving knots of gas called quasi-stationary flocculi (QSFs), which have been suggested to arise from the circumstellar bubble of the WN progenitor (Chevalier & Kirshner 1978).

Similarity solutions for SNRs mass-loaded from embedded clouds have been obtained by McKee & Ostriker (1977), Chièze & Lazareff (1981), and White & Long (1991) for conductively-driven evaporation, and by Dyson & Hartquist (1987) for ablation-driven injection. A small number of papers based on numerical simulations of mass-loaded supernova remnants also exist in the literature. Cowie, McKee & Ostriker (1981) included the dynamics of the clumps and found that warm clumps are swept towards the shock front and are rapidly destroyed, while cold clumps are more evenly distributed and have longer lifetimes. Arthur & Henney (1996) studied the effects of mass loading by hydrodynamic ablation on supernova remnants evolving inside cavities evacuated by the stellar winds of the progenitor stars.

When SNRs overlap in regions with vigorous star formation, they may create highly pressurized superbubbles that burst out into intergalactic space. In the standard picture of such starburst superwinds, the wind remains subsonic until it reaches the boundary of the starburst region (Chevalier & Clegg 1985). However, the predicted X-ray luminosity of the thermalized SN and stellar wind ejecta is lower than observed unless the superwind is heavily mass-loaded (Suchkov et al. 1996), with the rate of mass-injection from the destruction of clouds several times larger than that due to SNe (see also Hartquist et al. 1997). Recently, high-spatial-resolution observations have provided a much clearer view of the mass-loading process in superwinds. Cool $H\alpha$ emitting filaments and clumps are seen embedded within the superwind, and the soft X-ray emission appears to be associated with hot gas interacting with these structures (see Strickland et al. 2004, and references therein). Theoretical support comes from hydrodynamic models which show that the superwind sweeps up and incorporates large masses of material from within the galactic disk as it develops (Strickland & Stevens 2000).

Since superwinds are driven by overlapping SNRs, and the range and radiative energy losses of a remnant are affected by mass loading, it is desirable to have approximations which describe remnant evolution and range in clumpy media. The first steps towards this goal were taken by

Dyson, Arthur & Hartquist (2002) and Pittard et al. (2003), where hydrodynamical simulations of SNRs undergoing mass-loading driven either by ablation or conduction were calculated. Significant differences between the evolution of the SNRs were discovered, due to the way in which conductive mass loading is extinguished at fairly early times, once the interior temperature of the remnant falls below $\sim 10^7$ K. At late times, remnants that ablatively mass load are dominated by loaded mass and thermal energy, while those that conductively mass load are dominated by swept-up mass and kinetic energy. These works may ultimately be used in superwind models which are akin to the McKee & Ostriker (1977) model of the interstellar medium.

5.3 AGN-SNR Interaction

Many theoretical explanations have been proposed for the origin of the broad emission line regions (BELR) in AGNs (see, e.g., Pittard et al. 2003b, and references therein), including the interaction of an AGN wind with supernovae and star clusters (Perry & Dyson 1985; Williams & Perry 1994). It is now clear that the bulk of the broad-line emission arises from an accretion-disk wind (Proga, Stone & Kallman 2000, see also the chapter by Stuart Lumsden), but interactions between an AGN wind and SNRs may make a non-negligible contribution to the emission of high ionization lines. These interactions will also mass-load the AGN wind (e.g. Smith 1996), and possibly could be used as a diagnostic of it. Hydrodynamical simulations of the early stages of this interaction have been presented by Pittard et al. (2001c) and Pittard et al. (2003b). The strong radiation field means that cool post-shock gas forms only for a very limited time, before being heated back up to the Compton temperature.

5.4 Intracluster Gas

The intracluster medium consists of hot, subsonic gas which is bound within the gravitational potential of the cluster. It was suggested almost 3 decades ago that the density of gas within the central regions is high enough to permit significant cooling within a Hubble time. This energy loss causes outer gas to flow subsonically in to the centre in order to maintain hydrostatic equilibrium, a process referred to as a ‘cooling flow’. Recent X-ray observations appear to show a systematic deficit of low temperature emission in comparison to the standard isobaric cooling-flow model, which has led to the questioning of this model. Mass deposition rates significantly smaller than expected are also inferred (see, e.g., Peterson et al. 2003, and references therein). Attention has now focussed on the possibility that the gas is prevented from cooling by some compensating form of energy injection. For instance, the frequent occurrence of X-ray cavities coincident with radio lobes around the central dominant galaxy demonstrates that AGNs can significantly influence the X-ray morphology of

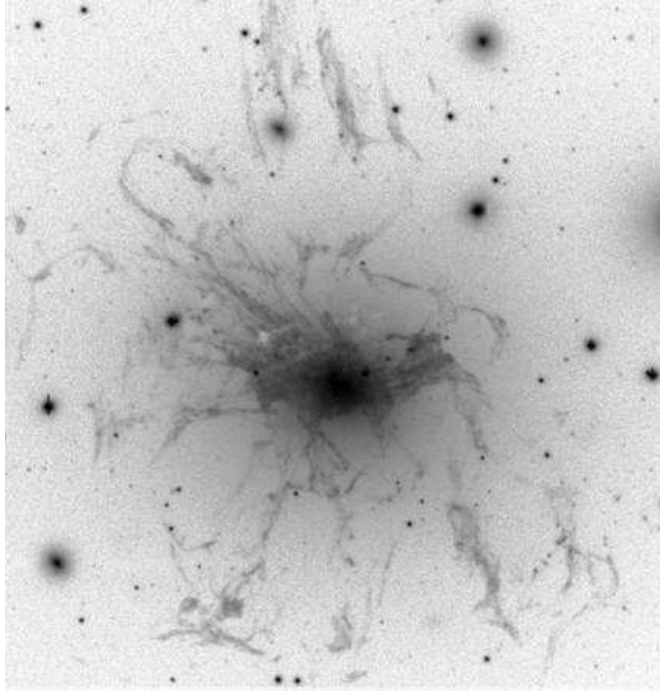


Fig. 7. An $H\alpha$ image showing the filamentary structure around NGC 1275 (credit C. Conselice (Caltech), WIYN, AURA, NOAO, NSF).

the hot gas (e.g., Fabian et al. 2002). However, the timescale for energy transfer from the relativistic plasma to the surrounding gas is poorly known, while the effectiveness of heat conduction at preventing cooling is enthusiastically debated.

An alternative interpretation is that the cooling plasma radiates its energy in the UV/optical bands rather than at X-ray wavelengths. This can occur if there is mixing between the cooling plasma and colder material (e.g., Fabian et al. 2002), and may be reprocessed into the IR if the gas is dusty. Luminous optical/UV nebulosity is common in cluster cooling flows (e.g., Heckman et al. 1989), and is particularly widespread around NGC 1275 in the Perseus cluster (Conselice, Gallagher & Wyse 2001) (see Fig. 7). While present information is rather sparse, and some of this emission will be powered by star formation, the total submillimetre to UV emission appears to be sufficient to account for the missing soft X-ray emission (Fabian et al. 2002). However, direct evidence for the UV emission resulting from this mixing is rather tentative in current FUSE data (Oegerle et al. 2001).

If cold clouds are embedded within the hot gas, they could be important for global mass injection into the hot surroundings. Indeed, since the intracluster gas is observed to be enriched with metals, material must either be injected by

the host galaxies, through fountain flows or superwinds, or ablatively stripped from them. Mass-loading usually reduces the mean temperature of a flow, as the thermal energy is shared between more particles, but in clusters this situation is modified by the gravitational forces on the flow and the significant gravitational potential energy that the entrained material possesses. A preliminary study has shown that under such conditions it is possible to increase the radiated power at high temperatures (Pittard et al. 2004). Hence the differential luminosity distribution can have a positive slope with T , as required for agreement with the latest observations of clusters. In addition, ripples found in the X-ray emission map of the Perseus cluster (Fabian et al. 2003) resemble the structure of some mass-loaded accretion flows. The most likely explanation for their origin may be time variations in the source of outflowing material, but this interaction clearly needs further investigation.

6 Summary

The mass-loading of flows is now recognized as a fundamental process in astronomy, yet much work remains. We still do not have a good understanding of ablatively-driven evaporation or conductively-driven thermal evaporation and the ability of plasma instabilities to quench it. The rapidity with which cold material is mixed into a hotter flow is also unknown. The global properties of a variety of mass-loaded flows have now been studied, but in only a few instances have specific objects been modelled and a direct comparison with observations made.

Acknowledgements

It is a pleasure to thank John Dyson for his encouragement and friendship, and to my other collaborators, Tom Hartquist and Sam Falle, for theirs.

References

- Arthur, S. J., Dyson, J. E., & Hartquist, T. W. 1993, *A&A*, 261, 425
- Arthur, S. J., Dyson, J. E., & Hartquist, T. W. 1994, *A&A*, 269, 1117
- Arthur, S. J., & Henney, W. J. 1996, *ApJ*, 457, 752
- Arthur, S. J., Henney, W. J., & Dyson, J. E. 1996, *A&A*, 313, 897
- Arthur, S. J., Lizano, S. 1997, *ApJ*, 484, 810
- Balbus, S. A. 1986, *ApJ*, 304, 787
- Balbus, S. A., & McKee, C. F. 1982, *ApJ*, 252, 529
- Bally, J., Sutherland, R. S., Devine, D., & Johnstone, D. 1998, *AJ*, 116, 293
- Bandiera, R., & Chen, Y. 1994a, *A&A*, 284, 629
- Bandiera, R., & Chen, Y. 1994b, *A&A*, 284, 637

- Bertoldi, F. 1989, *ApJ*, 346, 735
Bertoldi, F. 1990, *ApJ*, 354, 529
Böhringer, H., & Hartquist, T. W. 1987, *MNRAS*, 228, 915
Boroson, B., McCray, R., Clark, C. O., Slavin, J., Mac Low, M.-M., Chu, Y., & Van Buren, D. 1997, *ApJ*, 478, 638 [Erratum: 1997, *ApJ*, 485, 436]
Cantó, J., & Raga, A. C. 1991, *ApJ*, 372, 646
Chevalier, R. A., & Clegg, A. W. 1985, *Nature*, 317, 44
Chevalier, R. A., & Kirshner, R. P. 1978, *ApJ*, 219, 931
Chièze, J. P., & Lazareff, B. 1981, *A&A*, 95, 194
Cho, J., Lazarin, A., Honein, A., Knaepen, B., Kassinos, S., & Moin, P. 2003, *ApJ*, 589, L77
Chu, Y.-H. 1982, *ApJ*, 254, 578
Chu, Y.-H., Chang, H., Su, Y., & Mac Low, M.-M. 1995, *ApJ*, 450, 157
Chu, Y.-H., Guerrero, M. A., Gruendl, R. A., Williams, R. M., & Kaler, J. B. 2001, *ApJ*, 553, L69 [Erratum: 2001, *ApJ*, 554, 233]
Chu, Y.-H., Guerrero, M. A., Gruendl, R. A., García-Segura, G., Wendker, H. J. 2003, *ApJ*, 599, 1189
Chu, Y.-H., et al. 1999, *New Views of the Magellanic Clouds*, eds. Y.-H. Chu, N. Suntzeff, J. Hesser, & D. Bohlender, *IAU Symp.*, 190, 143
Conselice, C. J., Gallagher, J. S., & Wyse, R. F. G. 2001, *AJ*, 122, 2281
Cowie, L. L., & McKee, C. F. 1977, *ApJ*, 211, 135
Cowie, L. L., McKee, C. F., & Ostriker, J. P. 1981, *ApJ*, 247, 908
Cowie, L. L., & Songalia, A. 1977, *Nature*, 266, 501
David, L. P., & Durisen, R. H. 1989, *ApJ*, 346, 618
Draine, B. T., & Giuliani, J. L. 1984, *ApJ*, 281, 690
Dunne, B. C., et al. 2003, *ApJ*, 590, 306
Durisen, R. H., & Burns, J. O. 1981, *MNRAS*, 195, 535
Dyson, J. E. 1968, *Ap&SS*, 1, 388
Dyson, J. E. 1973, *A&A*, 23, 381
Dyson, J. E. 1992, *MNRAS*, 255, 460
Dyson, J. E. 1994, in *Lecture Notes in Physics*, 431, *Star Formation Techniques in Infrared and mm-Wave Astronomy*, ed. T. P. Ray & S. V. W. Beckwith (Berlin:Springer), 93
Dyson, J. E., Arthur, S. J., & Hartquist, T. W. 2002, *A&A*, 390, 1063
Dyson, J. E., & de Vries, J. 1972, *A&A*, 20, 223
Dyson, J. E., & Hartquist, T. W. 1987, *MNRAS*, 228, 453
Dyson, J. E., & Hartquist, T. W. 1994, *MNRAS*, 269, 447
Dyson, J. E., Hartquist, T. W., Pettini, M., & Smith, L. J. 1989, *MNRAS*, 241, 625
Dyson, J. E., Williams, R. J. R., & Redman, M. P. 1995, *MNRAS*, 237, 700
Elmegreen, B. G., & Lada, C. J. 1977, *ApJ*, 214, 725
Fabian, A. C., Allen, S. W., Crawford, C. S., Johnstone, R. W., Morris, R. G., Sanders, J. S., & Schmidt, R. W. 2002, *MNRAS*, 332, L50
Fabian, A. C., et al. 2003, *MNRAS*, 344, L43
Falle, S. A. E. G. 1975, *A&A*, 43, 323

- Falle, S. A. E. G., Coker, R. F., Pittard, J. M., Dyson, J. E., & Hartquist, T. W. 2002, *MNRAS*, 329, 670
- Ferrara, A., & Shchekinov, Y. 1993, *ApJ*, 417, 595
- Field, G. B. 1965, *ApJ*, 142, 531
- Fragile, P. C., Anninos, P., Gustafson, K., & Murray, S. D. 2005, *ApJ*, 619, 327
- Fragile, P. C., Murray, S. D., Anninos, P., & Breugel, W. V. 2004, *ApJ*, 604, 74
- Freyer, T., Hensler, G., & Yorke, H. W. 2006, *ApJ*, 638, 262
- Galeev, A. A., & Natanzon, A. M. 1984, *Dokl. Phys.*, 275, 6
- García-Segura, G., Langer, N., & Mac Low, M. M. 1996, *A&A*, 316, 133
- García-Segura, G., & Mac Low, M. M. 1995, *ApJ*, 455, 145
- Gary, S. P., & Feldman, W. C. 1977, *J. Geophys. Res.*, 82, 1087
- Giuliani, J. L. 1984, *ApJ*, 277, 605
- Grosdidier, Y., Moffat, A. F. J., Joncas, G., Acker, A. 1998, *ApJ*, 506, L127
- Hanami, H., & Sakashita, S. 1987, *A&A*, 181, 343
- Hartquist, T. W., & Dyson, J. E. 1988, *Ap&SS*, 144, 615
- Hartquist, T. W., Dyson, J. E., Pettini, M., & Smith, L. J. 1986, *MNRAS*, 221, 715
- Hartquist, T. W., & Dyson, J. E. 1993, *QJRAS*, 34, 57
- Hartquist, T. W., Dyson, J. E., & Williams, R. J. R. 1997, *ApJ*, 482, 182
- Heckman, T. M., Baum, S. A., van Breugel, W. J. M., & McCarthy, P. 1989, *ApJ*, 338, 48
- Hensler, G., & Vieser, W. 2002, *Ap&SS*, 281, 275
- Jun, B.-I., Jones, T. W., & Norman, M. L. 1996, *ApJ*, 468, L59
- Kahn, F. D. 1969, *Physica*, 41, 172
- Kastner, J. H., Balick, B., Blackman, E. G., Frank, A., Soker, N., Vrtílek, S. D., & Li, J. 2003, *ApJ*, 591, L37
- Kastner, J. H., Li, J., Vrtílek, S. D., Gatley, I., Merrill, K. M., & Soker, N. 2002, 581, 1225
- Klein, R. I., Budil, K. S., Perry, T. S., Bach, D. R. 2003, *ApJ*, 583, 245
- Klein, R. I., McKee, C. F., & Colella, P. 1994, *ApJ*, 420, 213
- Landau, L. D., & Lifshitz, E. M. 1959. *Fluid Mechanics*, Pergamon Press, Oxford
- Lefloch, B., & Lazareff, B. 1994, *A&A*, 289, 559
- Levinson, A., & Eichler, D. 1992, *ApJ*, 387, 212
- McKee, C. F., & Cowie, L. L. 1975, *ApJ*, 195, 715
- McKee, C. F., & Cowie, L. L. 1977, *ApJ*, 215, 213
- McKee, C. F., & Ostriker, J. P. 1977, *ApJ*, 218, 148
- Marcolini, A., Strickland, D. K., D'Ercole, A., Heckman, T. M., Hoopes, C. G. 2005, *MNRAS*, 362, 626
- Meaburn, J., Boumis, P., López, J. A., Harman, D. J., Bryce, M., Redman, M. P., & Mavromatakis, F. 2005, *MNRAS*, 360, 963
- Meaburn, J., Clayton, C. A., Bryce, M., & Walsh, J. R. 1996, *MNRAS*, 281, L57

- Meaburn, J., Nicholson, R. A., Bryce, M., Dyson, J. E., & Walsh, J. R. 1991, MNRAS, 252, 535
- Mellema, G., Kurk, J. D., & Röttgering, H. J. A. 2002, A&A, 395, L13
- Mellema, G., Raga, A. C., Cantó, J., Lundqvist, P., Balick, B., Steffen, W., & Noriega-Crespo, A. 1998, A&A, 331, 335
- O'Dell, C. R., Wen, Z., & Hu, X. 1993, ApJ, 410, 696
- Oegerle, W. R., et al. 2001, ApJ, 560, 187
- Orlando, S., Peres, G., Reale, F., Bocchino, F., Rosner, R., Plewa, T., Siegel, A. 2005, A&A, 444, 505
- Pavlakakis, K. G., Williams, R. J. R., Dyson, J. E., Falle, S. A. E. G., & Hartquist, T. W. 2001, A&A, 369, 263
- Perry, J. J., & Dyson, J. E. 1985, MNRAS, 213, 665
- Peterson, J. R., et al. 2003, ApJ, 590, 207
- Pittard, J. M., Arthur, S. J., Dyson, J. E., Falle, S. A. E. G., Hartquist, T. W., Knight M. I., & Pexon M. 2003, A&A, 401, 1027
- Pittard, J. M., Dyson, J. E., & Hartquist, T. W. 2001a, A&A, 367, 1000
- Pittard, J. M., Dyson, J. E., Falle, S. A. E. G., & Hartquist, T. W. 2001c, A&A, 375, 827
- Pittard, J. M., Dyson, J. E., Falle, S. A. E. G., & Hartquist, T. W. 2003b, A&A, 408, 79
- Pittard, J. M., Dyson, J. E., Falle, S. A. E. G., & Hartquist, T. W. 2005, MNRAS, 361, 1077
- Pittard, J. M., Hartquist, T. W., & Dyson, J. E. 2001b, A&A, 373, 1043
- Pittard, J. M., Hartquist, T. W., Ashmore, I., Byfield, A., Dyson, J. E., & Falle, S. A. E. G. 2004, A&A, 414, 399
- Poludnenko, A. Y., Frank, A., & Blackman, E. G. 2002, ApJ, 576, 832
- Proga, D., Stone, J. M., & Kallman, T. R. 2000, ApJ, 543, 686
- Rosner, R., & Tucker, W. H. 1989, ApJ, 338, 761
- Sandford, M. T. II, Whitaker, R. W., & Klein, R. I. 1982, ApJ, 260, 183
- Serabyn, E., Lacy, J. H., & Achtermann, J. M. 1991, ApJ, 378, 557
- Smith, L. J., Pettini, M., Dyson, J. E., & Hartquist, T. W. 1984, MNRAS, 211, 679
- Smith, L. J., Pettini, M., Dyson, J. E., & Hartquist, T. W. 1988, MNRAS, 234, 625
- Smith, S. J. 1996, ApJ, 473, 773
- Spitzer, L. 1962. Physics of Fully Ionized Gases, Interscience, New York
- Spitzer, L., & Härm, R. 1953, Phys. Rev., 89, 977
- Steffen, W., & López, J. A. 2004, ApJ, 612, 319
- Stone, J. M., & Norman, M. L. 1992, ApJ, 390, L17
- Strickland, D. K., Heckman, T. M., Colbert, E. J. M., Hoopes, C. G., & Weaver, K. A. 2004, ApJSS, 151, 193
- Strickland, D. K., & Stevens, I. R. 2000, MNRAS, 314, 511
- Suchkov, A. A., Berman, V. G., Heckman, T. M., Balsara, D. S. 1996, ApJ, 463, 528
- Toniazzo, T., Hartquist, T. W., & Durisen, R. H. 2001, MNRAS, 322, 149

- Townsley, L. K., Feigelson, E. D., Montmerle, T., Broos, P. S., Chu, Y.-H., & Garmire, G. P. 2003, *ApJ*, 593, 874
- Vieser, W., & Hensler, G. 2000, *Ap&SS*, 272, 189
- Warren, J. S., Hughes, J. P., & Slane, P.O. 2003, *ApJ*, 583, 260
- Weaver, R., McCray, R., Castor, J., Shapiro, P., & Moore, R. 1977, *ApJ*, 218, 377
- White, R. L., & Long, K. S. 1991, *ApJ*, 373, 543
- Williams, R. J. R. 2002, *MNRAS*, 331, 693
- Williams, R. J. R., & Dyson, J. E. 2002, *MNRAS*, 333, 1
- Williams, R. J. R., Dyson, J. E., & Hartquist, T. W. 1999, *A&A*, 344, 675
- Williams, R. J. R., Dyson, J. E., & Hartquist, T. W. 2000, *MNRAS*, 314, 315
- Williams, R. J. R., Hartquist, T. W., & Dyson, J. E. 1995, *ApJ*, 446, 759
- Williams, R. J. R., & Perry, J. J. 1994, *MNRAS*, 269, 538
- Wrigge, M. 1999, *A&A*, 343, 599
- Wrigge, M., Chu, Y.-H., Magnier, E. A., & Wendker, H. J. 2005, *ApJ*, 633, 248
- Xu, J., & Stone, J. M. 1995, *ApJ*, 454, 172
- Yusef-Zadeh, F., & Melia, F. 1992, *ApJ*, 385, L41
- Yusef-Zadeh, F., & Morris, M. 1991, *ApJ*, 371, L59
- Zhekov, S. A., & Myasnikov, A. V. 1998, *New Ast.*, 3, 57
- Zhekov, S. A., & Perinotto, M. 1996, *A&A*, 309, 648